Factors Influencing Deformations of Geocell-Reinforced Recycled Asphalt Pavement Bases under Cyclic Loading

Jitendra K. Thakur, P.E., M.ASCE[1]; Jie Han, P.E., F.ASCE[2]; and Robert L. Parsons, P.E., M.ASCE[3]

Abstract: A significant amount of recycled asphalt pavement (RAP) material is produced from flexible pavement rehabilitation projects. RAP can be used as a base course material for sustainable pavement construction. Performance of a pavement largely depends on the strength of its foundation, which consists of the subgrade and base course layers. Geocell was used in this study to increase the strength of RAP bases. Nine large-scale laboratory cyclic plate loading tests were conducted on unreinforced and geocell-reinforced RAP bases with three different thicknesses (150, 230, and 300 mm) over weak and moderate subgrades to investigate the influence of geocell confinement, base course thickness, base course strength, and subgrade strength on permanent and resilient deformations of RAP bases. The subgrade was prepared by mixing Kansas River sand with kaolin and compacted at weak [target California bearing ratio (CBR) = 2%] and moderate (target CBR = 5%) strengths. The test results showed that geocell confinement improved the performance of reinforced RAP bases by reducing permanent surface deformations and increasing resilient deformations and percentages of resilient deformation as compared with those of unreinforced bases. The RAP bases over the moderate subgrade performed better than those over the weak subgrade. Subgrade strength had a more pronounced effect than geocell confinement on the properties of RAP bases. Geocell confinement was more beneficial for the bases over the weak subgrade than those over the moderate subgrade. The relative improvement factors (RIFs) of the reinforced bases with respect to the unreinforced bases and the bases over the moderate subgrade with respect to the bases over the weak subgrade ranged from 1.1 to 11.4 and 1.2 to 17.2, respectively. The permanent deformation increased with the number of loading cycles and the RIFs increased with the permanent surface deformation of RAP base sections. **DOI: 10.1061/(ASCE)MT.1943-5533.0001760.**

Author keywords: Geocell; Reinforcement; Recycled asphalt pavement (RAP); Subgrade; Permanent deformation; Resilient deformation; Relative improvement factor.

Introduction

According to the National Asphalt Pavement Association (NAPA), the United States has more than 2.7 million km of paved roads, of which 94% are flexible pavements (NAPA 2016). Flexible pavements that have reached the end of their service life are frequently rehabilitated by removing existing asphalt surfaces and replacing the removed portion with new hot-mix asphalt (HMA). A large amount of recycled asphalt pavement (RAP) material is created every year during the rehabilitation and reconstruction of existing flexible pavements. RAP is obtained either by milling or a full-depth recovery method. Milling involves the mechanical removal of up to 50-mm-thick asphalt pavement in a single pass, whereas a full-depth recovery method uses a pneumatic pavement breaker or rhinoceros horn attached to a bulldozer to remove the entire asphalt pavement (Viyanant et al. 2007). According to the NAPA, the United States produced approximately 500 million t of asphalt pavement material each year. Surveys conducted by the North Carolina Department of Transportation (NCDOT) on behalf of the Federal Highway Administration (FHWA) and AASHTO in 2007 and 2009 showed that use of RAP was increasing across the nation (Copeland et al. 2010). Approximately 100 million t of RAP were used by different transportation agencies in the United States each year in the 2000s, compared with 72 million t used annually in the early 1990s (Copeland et al. 2010).

The FHWA supports the use of RAP as an alternative to virgin aggregate and asphalt in pavement construction. Papp et al. (1998) reported that use of RAP as a granular base material in pavement construction can be a sustainable option for pavement construction. According to the Recycled Material Research Center (2008), typical RAP contains 3–7% asphalt binder and 93–97% aggregate. Literature reveals that use of 100% RAP could not produce base course of high quality (Thakur and Han 2015). Several studies have been conducted in the past to improve the performance of RAP bases by blending RAP with virgin aggregates and stabilizing RAP using chemical additives (Abdelrahman et al. 2010; Attia 2010; Bennert et al. 2000; Bennert and Maher 2005; Clary et al. 1997; Cosentino et al. 2012; Garg and Thompson 1996; Guthrie et al. 2007; Kim and Labuz 2007; Li et al. 2007; Taha et al. 1999; Wen and Wu 2011; Wen et al. 2010). However, limited research has been conducted to investigate the performance of RAP stabilized with geosynthetics, especially geocell.

Clary et al. (1997), Bennert et al. (2000), Abdelrahman et al. (2010), and Cosentino et al. (2012) conducted resilient modulus (M_R) tests on RAP blended with aggregates and found that an increase of the virgin aggregate content in the blends reduced M_R and permanent deformation of blended samples. Li et al. (2007) and Wen et al. (2010) conducted M_R tests on fly ash–stabilized RAP samples and found that an increase of the fly ash content increased

[1]Staff Geotechnical Engineer, Terracon Consultants, Inc., 10400 State Highway 191, Midland, TX 79707. E-mail: erjkthakur@gmail.com

[2]Professor, Dept. of Civil, Environmental, and Architectural Engineering, Univ. of Kansas, 1530 W. 15th St., Lawrence, KS 66045-7609 (corresponding author). E-mail: jiehan@ku.edu

[3]Professor, Dept. of Civil, Environmental, and Architectural Engineering, Univ. of Kansas, 1530 W. 15th St., Lawrence, KS 66045-7609. E-mail: rparsons@ku.edu

Note. This manuscript was submitted on March 2, 2016; approved on July 26, 2016; published online on October 24, 2016. Discussion period open until March 24, 2017; separate discussions must be submitted for individual papers. This paper is part of the ***Journal of Materials in Civil Engineering***, © ASCE, ISSN 0899-1561.

M_R. Taha et al. (1999), Bennert and Maher (2005), Guthrie et al. (2007), and Cosentino et al. (2012) conducted California bearing ratio (CBR) tests on blended RAP samples and found that an increase of the virgin aggregate content in the blends increased CBR of blended samples. Li et al. (2007) conducted CBR tests on fly ash–stabilized RAP samples and found that an increase of the fly ash content increased the CBR value of fly ash–stabilized RAP. Garg and Thompson (1996), Bennert et al. (2000), Kim and Labuz (2007), Attia (2010), and Wen and Wu (2011) found that the permanent deformations of blended RAP aggregate specimens decreased with an increase of virgin aggregate in the blends. Wen et al. (2010) found that the fly ash–stabilized RAP specimens had lower permanent deformations than the virgin RAP specimens.

Mohammadinia et al. (2014) conducted a series of unconfined compression tests and repeated-load triaxial tests on cement-treated construction and demolition (C&D) materials, such as RAP, recycled concrete aggregate (RCA), and crushed brick (CB). They found that RAP showed highest strengths with the same cement content, curing period, and confining pressure followed by RCA and CB, and the resilient modulus of C&D materials increased with an increase of cement content, curing period, and confining pressure. Arulrajah et al. (2014) conducted large-scale direct shear tests on unreinforced and geogrid-reinforced C&D materials such as RAP, RCA, and CB and found that geogrid-reinforced RCA exhibited the highest interface peak and residual shear strengths followed by geogrid-reinforced CB and geogrid-reinforced RAP. Dong and Huang (2014) conducted repeated triaxial and creep tests on unbound RAP, crushed limestone, and crushed gravel with the same gradation and prepared at the same compaction level. They found that unbound RAP exhibited higher resilient modulus, permanent deformation, and creep deformation compared with crushed limestone and gravel. They also suggested not to use unbound RAP as a base material in construction of asphalt pavement. Thakur and Han (2015) summarized the recent development of RAP bases treated for highway construction.

Geosynthetics, including geocells, have been used to improve the performance of unpaved and paved roads (Han 2015). Most studies on geocell reinforcement to date have been based on sand or aggregate as infill materials. Very limited studies (Han et al. 2011; Bortz et al. 2012; Thakur et al. 2012, 2013) have been conducted on geocell-reinforced RAP bases and indicated that three-dimensional polymeric geosynthetic cells, commonly known as geocells, can be successfully used to improve the performance of RAP bases. Thakur et al. (2013) conducted medium-scale laboratory static plate loading tests on unreinforced and geocell-reinforced RAP bases over rigid subgrade to investigate the benefits of geocell confinement on creep deformation behavior and stiffness of geocell-reinforced RAP bases. They concluded that geocell confinement increased the stiffness and reduced the creep deformation of the RAP bases. Bortz et al. (2012) conducted moving wheel tests on asphalt pavements with unreinforced and geocell-reinforced bases with different infill materials. They concluded that geocell-reinforced RAP bases performed as well as the geocell-reinforced well-graded aggregate base. They also found that pavements constructed over a strong subgrade performed better than those constructed over a weak subgrade. Han et al. (2011) conducted moving wheel tests on unpaved roads with unreinforced and geocell-reinforced RAP bases and found that the geocell reduced the rut depth and vertical stress transferred to the subgrade by distributing the load over a wider area. However, moving wheel tests are costly and only a limited number of tests can be performed.

Han et al. (2012) conducted large-scale cyclic plate loading tests on asphalt pavements with unreinforced and geocell-reinforced RAP bases over moderate subgrade. Thakur et al. (2012) conducted large-scale laboratory cyclic plate loading tests on unreinforced and geocell-reinforced RAP bases over weak subgrade and concluded that geocell improved the performance of RAP bases by reducing the surface permanent deformation and vertical stress at the interface of base and subgrade, and by increasing the percentage of resilient deformation. They found that the geocell-reinforced RAP bases showed a stable response, whereas the unreinforced RAP base showed an unstable response. Han and Thakur (2015) summarized the recent research on the sustainable roadway construction using recycled aggregates with geosynthetics. They also reported that geocell-reinforced RAP used as base course material is a sustainable pavement construction technology.

However, no study has been conducted to investigate the effect of subgrade strength on the performance of geocell-reinforced RAP bases under cyclic loading. In this study, four cyclic plate loading tests were conducted on unreinforced and reinforced RAP bases over weak subgrade (target CBR = 2%) while five cyclic plate loading tests were conducted on unreinforced and geocell-reinforced RAP bases over moderate subgrade (target CBR = 5%). These tests were conducted in a large test box to investigate the benefits of geocell confinement, base thickness, and base and subgrade strengths in improving the performance of RAP bases. The improvement in the performance is presented in terms of reduction in the permanent surface deformation and increase in the resilient deformation. The reduction in permanent deformation is presented in terms of relative improvement factor (RIF).

Table 1. Properties of the RAP Materials Used in This Study

Property	Value	Test method
Bulk specific gravity		
Fine aggregate	2.48	ASTM C128 (ASTM 2007c)
Coarse aggregate	2.39	ASTM C127 (ASTM 2007b)
Apparent specific gravity		
Fine aggregate	2.69	ASTM C128 (ASTM 2007c)
Coarse aggregate	2.60	ASTM C127 (ASTM 2007b)
Saturated surface dry (SSD) bulk specific gravity		
Fine aggregate	2.56	ASTM C128 (ASTM 2007c)
Coarse aggregate	2.49	ASTM C127 (ASTM 2007b)
Uncompacted void content (%)		
Fine aggregate	39.15	ASTM C1252 (Method B) (ASTM 2006)
Mean particle size (d_{50}) (mm)	2.0	—
Coefficient of curvature (C_c)	0.85	—
Coefficient of uniformity (C_u)	8.33	—
Asphalt binder		
Binder content (%)		
Centrifuge method	6.71	ASTM D2172 (ASTM 2011)
Ignition method	6.87	ASTM D6307 (ASTM 2010)
Viscosity of asphalt binder at 135°C (Pa · s)	1.408	ASTM D1856 (ASTM 2009b)

Test Materials

Base Material

RAP material brought from R.D. Johnson Excavating, (Lawrence, Kansas) was used as the base course layer for all test sections. The properties of the RAP material were determined by laboratory tests following different ASTM standards and are presented in Table 1. The fine and coarse aggregates were extracted from RAP by an ignition method, whereas asphalt was extracted by a centrifuge method for determining its properties. Fig. 1 shows the gradation curve of the RAP aggregate extracted by the ignition

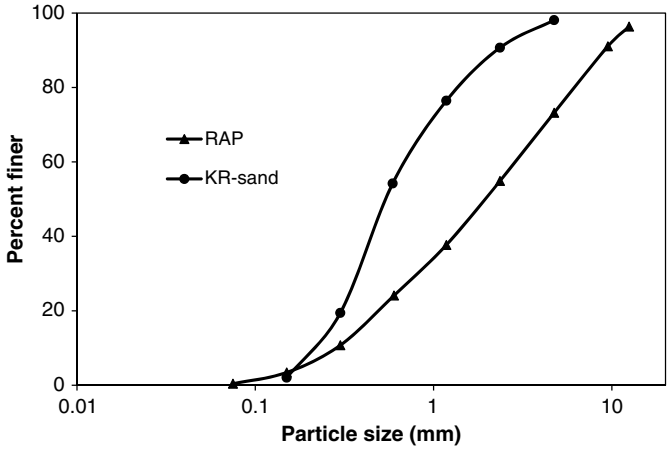

Fig. 1. Gradation curves

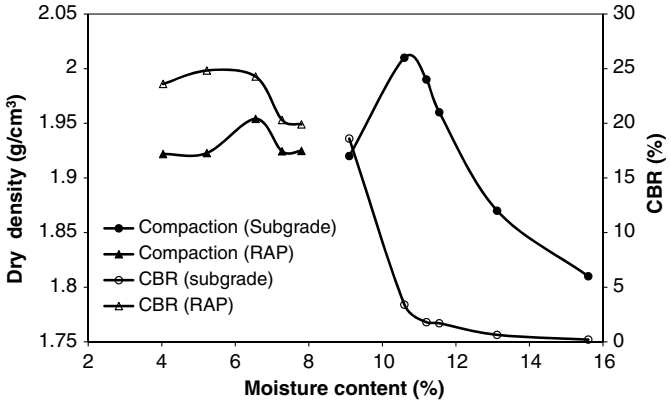

Fig. 2. CBR and compaction curves (modified from Thakur et al. 2012)

method. The modified Proctor compaction and unsoaked CBR curves for RAP are shown in Fig. 2. The RAP had a maximum dry density of approximately 1.96 g/cm^3 at an optimum moisture content of 6.6%, and a CBR value of 24.8% at 5.3% moisture content and a CBR value of 24.2% at its optimum moisture content.

Subgrade

A mixture of 25% kaolin and 75% Kansas River (KR) sand was used as a subgrade layer for all test sections. The poorly graded subrounded KR sand had a mean particle size $(d_{50}) = 0.54$ mm, coefficient of curvature $(C_c) = 0.95$, coefficient of uniformity $(C_u) = 3.1$, and specific gravity = 2.62 (Pokharel et al. 2010). Fig. 1 shows the gradation curve of the KR sand. The liquid and plastic limits of the subgrade soil were found to be 30 and 22%, respectively. The standard Proctor compaction and unsoaked CBR curves of the subgrade with moisture content (%) are shown in Fig. 2. The subgrade had a maximum dry density of approximately 2.01 g/cm^3 at an optimum moisture content of 10.8%, and a CBR value of 2% at 11.4% moisture content and a CBR value of 5% at 10.4% moisture content.

Geosynthetics

A novel polymeric alloy (NPA) geocell and a 99.65-g nonwoven geotextile were the two types of geosynthetics used in this study. The geocell was used for RAP base stabilization, whereas the geotextile was used at the interface of base and subgrade as a separator in all the reinforced test sections. The geocell provided by PRS Mediterranean Ltd. (Tel-Aviv, Israel) had a wall thickness of 1.1 mm, heights of 100 and 150 mm, and two holes of 100-mm^2 area on each pallet. The properties of the geocell and the geotextile are provided in Table 2 and were same as those reported in Thakur et al. (2012).

Test Equipment

Large-scale cyclic plate loading tests were conducted in a steel box in the geotechnical laboratory at the University of Kansas. The

Table 2. Material Properties of the NPA Geocell and Geotextile (Data Courtesy of PRS Mediterranean, Ltd.)

Geosynthetics	Properties	Value	Unit	Test method
NPA geocell	Tensile strength	>20	N/mm	PRS method
	Tensile modulus at 1% strain	462	N/mm	—
	Allowed strength for design of 50 years	>5.7	N/mm	ASTM D6992 (ASTM 2009a)
	Creep reduction factor	<3.5	—	ASTM D6992
	Coefficient of thermal expansion (CTE)	≤80	parts per million (ppm)/°C	ISO 11359-2 (ASTM 1999) ASTM E831 (ASTM 2014a)
			Flexural storage modulus at	
	30°C	>750	MPa	ISO 6721-1 (ASTM 2011)
	45°C	>650		ASTM E2254 (ASTM 2013c)
	60°C	>550		
	80°C	>300		
	Oxidative induction time (OIT)	≥100	min	ISO 11357-6 (ASTM 2006) ASTM D3895 (ASTM 2014b) (OIT at 200°C, 25 kPa)
	Durability of ultraviolet degradation	≥400	min	ASTM D5885 (2015b) [High pressure oxidative induction time (HPOIT) at 150°C, 3,500 kPa]
Geotextile	Grab tensile strength	0.401	kN	ASTM D4632 (ASTM 2015a)
	Grab elongation	50	%	ASTM D4632
	Trapezoid tear strength	0.178	kN	ASTM D4533 (ASTM 2015c)
	Puncture resistance	0.267	kN	ASTM D4833 (ASTM 2013b)
	Mullen burst strength	1378	kPa	ASTM D3786 (ASTM 2013a)
	Permittivity	2.2	1/s	ASTM D4491 (ASTM 2016c)
	Water flow	6095	1/min/m^2	ASTM D4491
	Apparent opening size (AOS)	0.212	mm	ASTM D4751 (ASTM 2016a)

overall dimensions of the box were 2.2 m long, 2 m wide, and 2 m high. Unpaved road test sections were constructed inside the box. The bottom and three sides of the box were fixed by steel plates, which were reinforced with square steel tubing. The front of the box had detachable steel channel sections 150 mm high, which were fixed with nuts and bolts to permit the construction of test sections. A servohydraulic MTS (Eden Prairie, Minnesota) loading system was used to apply a cyclic load on test sections in the box. The loading system consisted of a loading frame, a hydraulic actuator, and a servo-control unit. A hydraulic actuator with a load capacity of 245 kN was used to apply a cyclic load on the steel loading plate that was seated on the surface of a test section. This cyclic load wave had a 2.0-s initial period in which a small load of 0.5 kN was held constant, followed by a linear load increase from 0.5 to 40 kN over a 0.3-s rise time, followed by a 0.2-s period in which the load was held constant, followed by a linear load decrease from 40 to 0.5 kN over 0.3 s, and finally followed by a 0.5-s period of 0.5 kN load before the load cycle was repeated. This load wave had a frequency of 0.77 Hz. The loading plate connected to the actuator was 300 mm in diameter and 30 mm thick. A 10-mm-thick rubber pad was attached to the bottom of the loading plate to ensure full contact with the base and minimize stress concentration at the edge of the plate. The initial 2-s period represents the application of the seating load. The peak load of 40 kN and the loading plate 300 mm in diameter were used in cyclic load tests to simulate a single wheel load (equivalent to an axle load of 80 kN and a tire contact pressure of 550 kPa). The tire pressure of 550 kPa is commonly used in practice to represent a truck wheel on roadways. Qian et al. (2011), Han et al. (2012), and Thakur et al. (2012) have used the same loading wave to conduct cyclic loading tests. A servocontrol unit was connected to a data acquisition system and a hydraulic control valve.

Test Section Preparation

Nine unpaved road test sections were prepared in the large test box. Four (one unreinforced and three geocell-reinforced) and five (two unreinforced and three geocell-reinforced) bases were prepared over weak (target CBR = 2%) and moderate (target CBR = 5%) subgrade, respectively. Each test section included a 1.0-m-thick subgrade soil layer prepared and compacted by a vibratory plate compactor in eight lifts (150 mm each for the bottom 600-mm-thick subgrade and 100 mm each for the remaining 400-mm-thick subgrade) at 11.4 and 10.4% moisture contents to obtain target CBR values of 2 and 5%, respectively. The subgrade strength was checked by vane shear testing [ASTM 4648-05 (ASTM 2016b)] during the subgrade preparation. According to ASTM 4648-05, torque was applied at a rotation rate of 60 to 90°/min to the vane during testing. The vane shear test device directly measured the undrained shear strength (C_u) of the subgrade, and then the subgrade CBR was estimated by using the correlation CBR = $C_u/20.5$ (Pokharel et al. 2010), where C_u is the undrained shear strength of subgrade in kilopascals. After preparation of the subgrade at the desired CBR, four strain gauge–type earth pressure cells 11.3 mm thick with 50 mm outer diameter, 46 mm sensing area diameter, and 160 g weight were installed on top of the subgrade. The earth pressure cells having the maximum capacities of 500, 500, 250, and 250 kPa were installed at the center and 12.5, 25, and 50 mm away from the center of the loading plate, respectively.

The reinforced bases constructed over weak and moderate subgrade were 150, 230, and 300 mm thick. The unreinforced bases constructed over moderate subgrade were 150 and 300 mm thick, while that constructed over weak subgrade was 300 mm thick. For the 150- and 300-mm-thick unreinforced RAP base, RAP was placed on top of the subgrade and compacted by a vibratory plate compactor in lifts (100 or 50 mm each). A layer of geotextile was placed on the top of the subgrade in the reinforced sections. For the 150- and 230-mm-thick reinforced RAP bases, 100- and 150-mm-high geocells were installed on the top of the geotextile, respectively, and then were filled with RAP and compacted by hand tamping inside each cell. A RAP cover approximately 50 or 80 mm thick was added on the filled geocell for the 150- or 230-mm-thick section for the protection of geocells. The cover material was compacted by the vibratory plate compactor. Similarly, the 300-mm-thick reinforced base was prepared in four lifts and two geocell layers (i.e., 100-mm-high geocell plus a 30-mm-thick cover and 100-mm-high geocell plus a 70-mm-thick cover). There are common heights of geocells used in practice. The required base thickness can be maintained by changing the cover thickness and the cell height. Fixing the cover thickness may result in a geocell height that is not available for products in the market. In this study, the cover thickness of 30–80 mm was chosen to simulate the thickness of base course usually used in the field, such as 150, 230, and 300 mm. For each test section, the RAP material of each lift was compacted to a target density corresponding to 95% of the maximum dry density on the drier side of the compaction curve within 2% range of moisture content. The quantities (weights) of subgrade and RAP materials for each lift were calculated by multiplying the moist density of the material by the volume of each lift to fill in the box.

The strengths of subgrade and base course were determined by conducting dynamic cone penetration (DCP) tests 1 day after the preparation of the base course. The CBR values of subgrade and base course were estimated by using the correlation CBR = $292/(\text{PI})^{1.12}$ (Webster et al. 1994), where PI represents the penetration index in millimeters per blow (calculated based on the amount of penetration per blow). The amount of penetration for each blow was measured in millimeters and is noted here as penetration index (PI). The CBR values at different depths were calculated using the aforementioned correlation and then the average CBR was calculated and reported in Table 3. The density of the base course was also verified by conducting sand cone tests after the plate loading test.

Instrumentation

Five strain gauge–type displacement transducers manufactured by Tokyo Sokki Kenkyujo, (Tokyo, Japan) were used to measure surface deformations of the RAP bases. Two transducers with a 100-mm range were installed on the loading plate, one with a 100-mm range was installed 250 mm away from the center, and two displacement transducers with a 50-mm range were installed 500 and 750 mm away from the center of the loading plate,

Table 3. Test Sections and Their CBR and Relative Compaction Values

Test sections	Subgrade undrained shear strength, C_u (kPa) (vane shear test result)	Subgrade CBR (%) (vane shear/DCP)	Base CBR (%)	Relative compaction (%)
150 mm R_W	43.1	2.1/2.8	11.4	93
230 mm R_W	39.0	1.9/2.1	6.3	84
300 mm R_W	41.0	2.0/2.1	10.2	91
300 mm UR_W	39.0	1.9/2.0	10.2	91
150 mm R_M	98.4	4.8/4.8	10.4	87
230 mm R_M	94.3	4.6/4.7	10.5	91
300 mm R_M	92.3	4.5/4.6	10.2	89
150 mm UR_M	98.4	4.8/5.0	10.5	96
300 mm UR_M	92.3	4.5/4.6	11.4	88

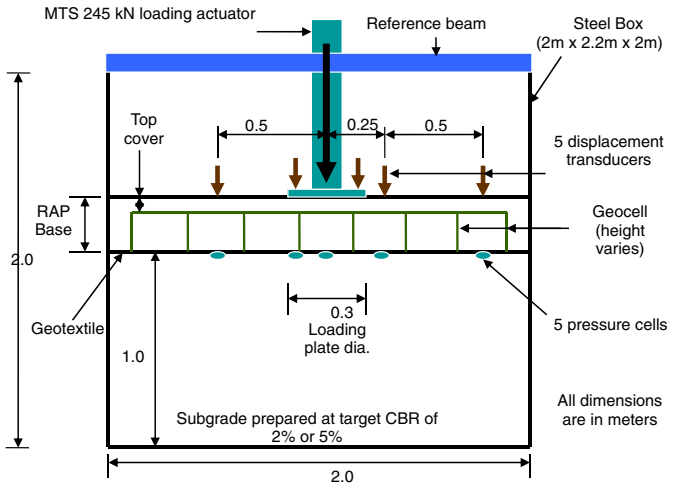

Fig. 3. Schematic diagram for the setup of cyclic plate load test

respectively. The transducers installed away from the center were seated on small metal plates placed on the top of the base course. All the transducers were mounted on a steel reference beam set at the top of the test box as shown in Fig. 3. The vertical stresses at the interface of subgrade and base course and the surface deformations were measured by pressure cells and displacement transducers, respectively. Four smart dynamic strain data recorders (Model DC-204R, Tokyo Sokki Kenkyujo, Tokyo, Japan) were used to record the data measured by all sensors. One recorder was used as a master while the other three served as slaves and were synchronized with the master recorder. A total of 16 connection ports (four on each recorder) were available for recording data. The accuracies of earth pressure cells and displacement transducers were 0.001 kPa and 0.01 mm, respectively. The test box, the loading type, the loading system, and the instrumentation were the same as those used by Thakur et al. (2012). This paper will focus on the analysis of the deformation data measured by the displacement transducers. The 300-mm-thick reinforced base over weak subgrade and the 300-mm-thick unreinforced base over weak subgrade sections are represented by 300 mm R_W and 300 mm UR_W, respectively, while the 300-mm-thick reinforced base over moderate subgrade and the 300-mm-thick unreinforced base over moderate subgrade sections are represented by 300 mm R_M and 300 mm UR_M, respectively. Similar representation also holds for other remaining sections for ease of presentation.

Test Results and Discussions

Quality Control Test Results

The required strengths of base and subgrade layers were checked by conducting five vane shear tests at five different locations just after preparation of a subgrade and four DCP tests at four different locations 1 day after the preparation of a base course within the test box. After each cyclic plate loading test, two sand cone tests [ASTM D1556-07 (ASTM 2007a)] were conducted outside the loaded area to evaluate the density of the compacted RAP base. The CBR values of subgrade and base layers were calculated from vane shear and DCP test data using the correlations provided in the previous section. The CBR profiles obtained from DCP tests for all test sections are shown in Figs. 4(a–c). A summary of shear strengths of subgrade, average CBR values of the base and the subgrade, and relative compaction of the base for all unreinforced and

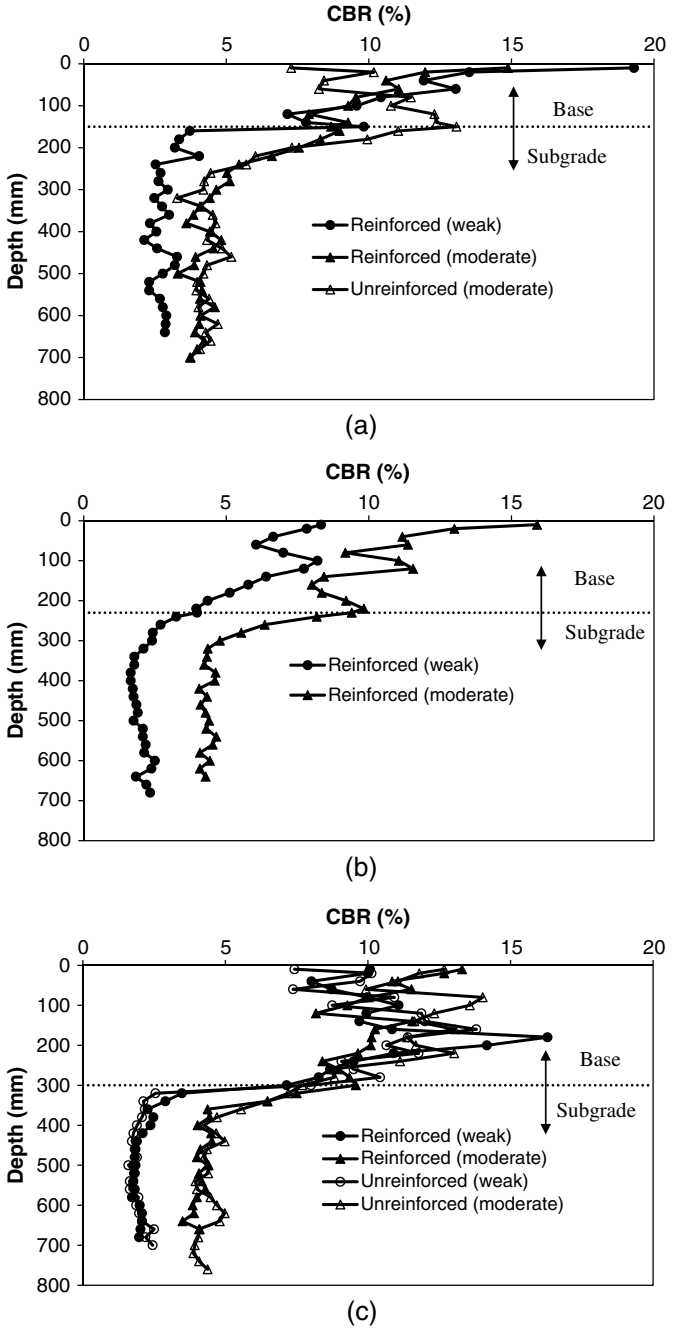

Fig. 4. CBR profiles obtained from DCP tests: (a) 150-mm-thick base; (b) 230-mm-thick base; (c) 300-mm-thick base

reinforced test sections are presented in Table 2. The average CBR values of the subgrade obtained from the DCP tests were slightly higher than those from the vane shear tests. This may be because the DCP tests were conducted 1 day after the preparation of test sections. Average CBR values of each base course ranged from 10.2 to 11.4% except the 230-mm-thick reinforced base over weak subgrade. The standard deviations for the CBR and the relative compaction ranged from 0.23 to 1.4% and 0.2 to 2.9%, respectively. The 230-mm-thick reinforced base over the weak subgrade had a lower CBR value because of inadequate compaction. The moisture content of RAP base material used in the 230 mm R_W section was approximately 1.3% lower than the target moisture content. The authors believe this inadequate compaction was due to inadequate moisture content in the RAP base material. The

less-compacted 230-mm-thick reinforced base course over weak subgrade had poorer performance than other sections, which will be discussed subsequently.

Permanent Surface Deformation

Thompson and Smith (1990) reported permanent deformation or rutting as the most common criterion to determine the performance of roads. The total surface deformations for each loading cycle were measured by the displacement transducers installed on top of the prepared sections. The total deformation consisted of permanent and resilient deformations. The permanent and resilient deformations for each loading cycle were separated from the total deformation and are presented separately in this paper. The permanent deformation of the loading plate reaching at least 75 mm was used as the criterion to terminate each cyclic loading test. This criterion was used by Hammitt (1974) and Giroud and Han (2004a, b) to define the failure of unpaved roads. The permanent surface deformation at the center of the loading plate was calculated by averaging the permanent deformation values recorded using two displacement transducers installed on top of the loading plate, while the permanent surface deformations at the locations away from the center of loading plate were kept the same as those recorded by the displacement transducers installed at each particular location. The permanent surface deformations at the center of the loading plate versus the number of loading cycles for 150-, 230-, and 300-mm-thick bases over weak and moderate subgrade are shown in Figs. 5(a–c), respectively. The permanent deformation increased with the number of loading cycles. The rate of increase in the permanent deformation decreased with an increase in the number of loading cycles. All geocell-reinforced sections had lower permanent deformations and rates of increase in permanent deformations than the corresponding thick unreinforced sections under the similar condition of construction. The thicker base sections had lower permanent deformations than thinner bases under similar conditions of construction. The surface permanent deformation was mostly contributed by the weak subgrade. Thakur et al. (2012) showed that the vertical stress at the interface of subgrade and base course was lower for the thicker section than the thinner section. Therefore, the thicker section resulted in smaller surface permanent deformations than the thinner section. The 230 mm R_W experienced higher permanent deformations than the 150 mm R_W. This result was due to the lower CBR value of the base resulting from less compaction in the 230 mm R_W section. The sections constructed over the moderate subgrade had lower permanent deformations than those over weak subgrade. The unreinforced bases over the moderate subgrade had lower permanent deformations than the corresponding thick reinforced bases over the weak subgrade. This indicates that geocell confinement and subgrade strength played vital roles in improving the performance of test sections. The subgrade strength had a more significant effect than the geocell confinement in reducing permanent surface deformations.

Relative Improvement Factor

To demonstrate the effects of different influence factors on the improved performance of road sections, a relative improvement factor is introduced in this paper. The RIF is calculated by the ratio of the number of loading cycles for the strong section at a certain permanent deformation to that for the weak section at the same permanent deformation. The RIF versus permanent deformation curves were plotted to demonstrate the influence of four factors (i.e., base thickness, geocell reinforcement, base strength, and subgrade strength) on the improved performance of unpaved roads with RAP bases.

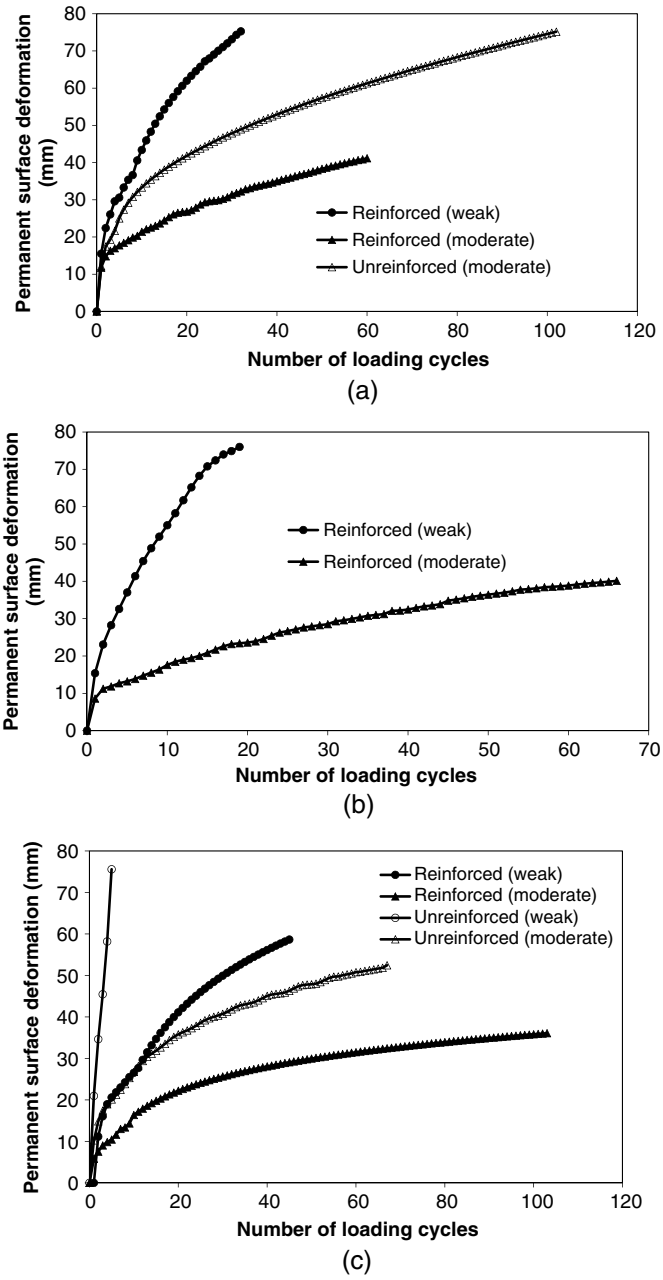

Fig. 5. Permanent surface deformation at the center of the loading plate versus the number of loading cycles: (a) 150-mm-thick base; (b) 230-mm-thick base; (c) 300-mm-thick base

To demonstrate the effect of one factor on the RIF, the other three factors were held constant.

Effect of Base Thickness

Fig. 6 presents the RIF versus permanent surface deformation curves for the 300-mm-thick unreinforced or reinforced base sections relative to the 150-mm-thick unreinforced or reinforced base sections to demonstrate the benefit of an additional 150 mm of RAP material. The RIF values of 300 mm R_W, 300 mm R_M, and 300 UR_M sections were calculated with respect to 150 mm R_W, 150 mm R_M, and 300 UR_M sections, respectively. The test results showed that an additional 150 mm of RAP material improved the performance of test sections by a factor of 1.1 to 2.7. All test sections had the largest RIF values at the highest

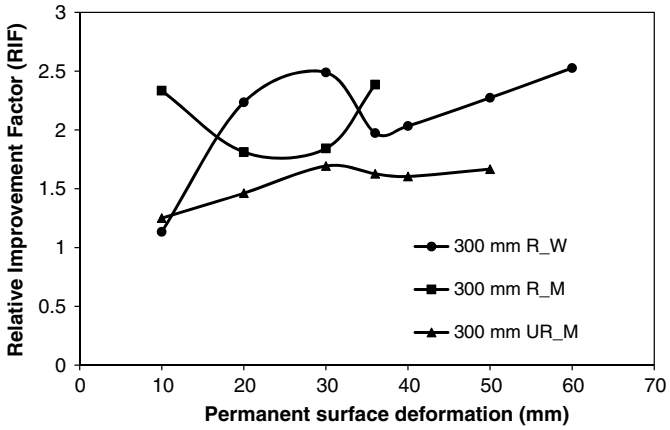

Fig. 6. Effect of base course thickness on RIF relative to 150-mm-thick base courses

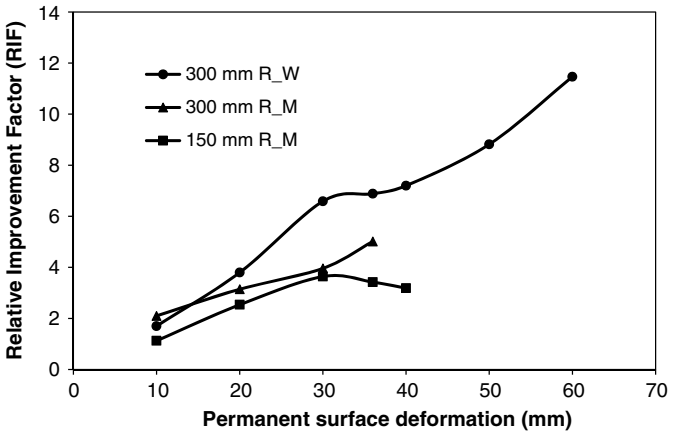

Fig. 7. Effect of geocell reinforcement on RIF relative to unreinforced base courses

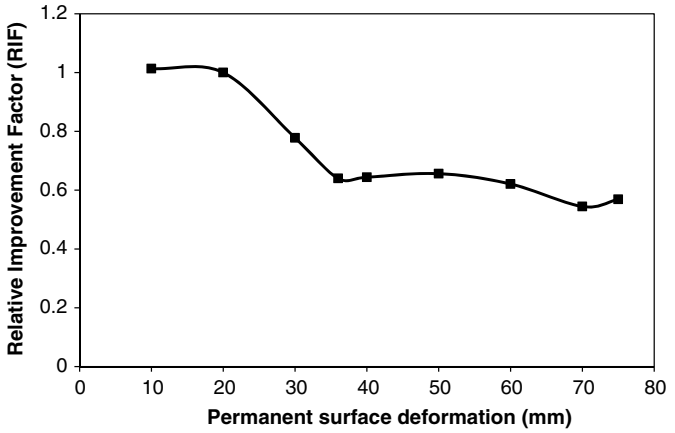

Fig. 8. Effect of base course strength on RIF (230-mm reinforced base course over weak subgrade relative to 150-mm reinforced base course over weak subgrade)

permanent deformations. The amount of the permanent deformation of the thin reinforced section increased rapidly during the first few loading cycles and then increased at a reduced rate after the geocell was mobilized. However, the permanent deformation of the thick reinforced section increased at a slower rate than the thin section during the first few loading cycles, then at a faster rate than the thin section until the geocell in the thick section was mobilized and then at a slower rate again after the geocell was mobilized. Thus the 300 mm R_W section shows an increase-decrease-increase trend, whereas the 300 mm UR_M section shows an increase-decrease-constant trend. In addition, the base CBR in the 150 mm R_M section was a little higher than that in the 300 mm R_M section. The 150 mm R_M section deformed at a slower rate during the first few loading cycles than the 300 mm R_M section and therefore the 300 mm R_M section shows a decrease-increase trend.

Effect of Geocell Reinforcement

Fig. 7 presents the RIF versus permanent surface deformation curves for the 150- and 300-mm-thick reinforced base sections relative to the unreinforced base sections of the same thickness. The 150- and 300-mm-thick reinforced base sections consisted of one layer and two layers of 100-mm-high geocells, respectively. The test results showed that the geocell-reinforced bases improved the performance of the test sections by a factor of 1.1 to 11.4 relative to the corresponding unreinforced base sections. The reinforced sections with two layers of geocell had higher RIFs than the section with one layer of geocell. The RIF increased with an increase of the permanent deformation. This phenomenon is because the contribution of the geocell was more mobilized at a larger permanent deformation and improved the performance by the mechanism of the beam or tensioned membrane effect of the geocell-reinforced bases as reported by Thakur et al. (2012). Thakur et al. (2012) also indicated that the 150-mm-thick reinforced base behaved as a tensioned membrane, while the 300-mm-thick reinforced base behaved as a slab with bending resistance and the 230-mm-thick reinforced base behaved as a slab first and then a tensioned membrane.

Effect of Base Course Strength

It would be ideal if two test sections had the same conditions except for the base course strength to investigate the effect of base course strength. These test sections did not exist in this study, so the performance of the thicker reinforced section with the lower base course strength (230 mm R_W) was compared with that of the thinner reinforced section with the higher base course strength (150 mm R_W) to demonstrate the effect of the base course strength. The CBR values of the base course for 150 mm R_W and 230 mm R_W sections were 11.4 and 6.3%, respectively. Fig. 8 presents the RIF versus permanent surface deformation curve for the 230 mm R_W section relative to the 150 mm R_W section. Even though the 230 mm R_W section was thicker than the 150 mm R_W section, the RIF of the 230 mm R_W section relative to the 150 mm R_W section ranged from 0.5 to 1.0. This result indicated that the 230 mm R_W section performed more poorly than the 150 mm R_W section. In other words, the strength of the base course played a more important role in the improved performance than the thickness of base course.

Effect of Subgrade Strength

Fig. 9 presents the RIF versus permanent surface deformation curves for the 150-, 230-, and 300-mm-thick reinforced bases and the 300-mm-thick unreinforced bases over moderate subgrade relative to weak subgrade. The RIFs increased with the permanent deformation. The test results showed that the RAP bases over the moderate subgrade withstood 1.2–17.2 times the number of cycles the corresponding bases over the weak subgrade did for the same deformations. From the measurements of vertical stresses

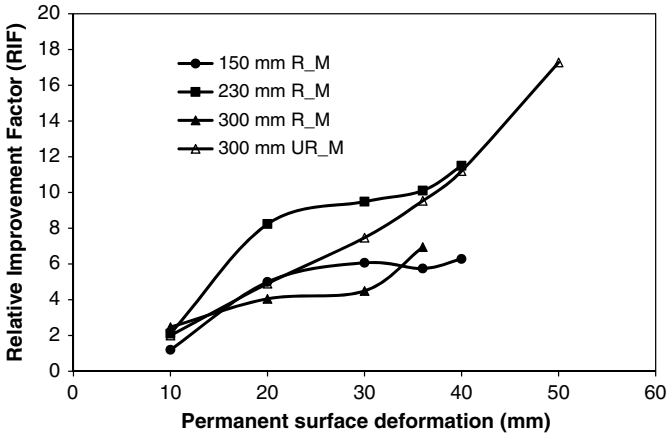

Fig. 9. Effect of subgrade strength on RIF relative to base courses over weak subgrade

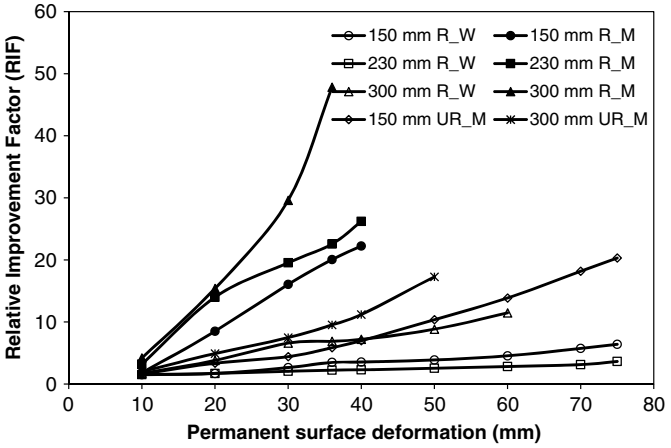

Fig. 10. Overall RIF relative to the 300-mm-thick unreinforced base over weak subgrade

at the interface of base course and subgrade, Thakur et al. (2013) found that the section prepared over moderate subgrade showed more stable response than that over weak subgrade. Thus, the moderate subgrade provided better support for the overlying base course layer than the weak subgrade and improved the performance of the test sections. The improvement depends on the deformations of the RAP base and the subgrade and the slab or tensioned membrane effect. Due to the combined effect, the exact reason for the amount of improvement for each test section is unknown. Numerical analysis is needed to separate the contribution by each component.

Overall Performance

A total of nine unreinforced and geocell-reinforced sections with three different base course thicknesses (150-, 230-, and 300-mm-thick base sections) and two different subgrade strengths (target CBR of subgrade = 2 and 5%) were compared with the weakest section (300 mm UR_W) to demonstrate the effect of the base course thickness, the geocell reinforcement, the subgrade strength, and the base course strength, among other things. The 300 mm UR_W section had the highest permanent deformations for the particular loading cycles and was considered the weakest section among all nine sections. The RIF value of each test section was calculated relative to the 300 mm UR_W section to determine the overall relative performance. Fig. 10 shows the RIF versus permanent deformation curve to demonstrate the relative performance of each test section with respect to the weakest test section (i.e., the 300 mm UR_W section). The test result showed that the 300 mm R_M section performed best, followed by the 230 mm R_M, 150 mm R_M, 300 mm UR_M, 150 mm UR_M, 300 mm R_W, 150 mm R_W, 230 mm R_W, and 300 mm UR_W sections. The 150 mm R_W section performed better than the 230 mm R_W section due to less compaction of the 230 mm R_W section resulting in a lower CBR value of the base in the 230 mm R_W section compared with that in the 150 mm R_W section. The degree of improvement shown in Fig. 10 was due to the combined effect of the base course thickness, the geocell reinforcement, and the base and sugrade strengths. The RIF values for all test sections ranged from 1.6 to 47.8.

Permanent Surface Deformation Profile

Figs. 11(a–c) show the permanent surface deformation profiles at the fifth loading cycle constructed using the deformation data recorded by five displacement transducers installed at the center of the loading plate and 250, 500, and 750 mm away from the center of the loading plate. The surface deformation profiles were assumed to be symmetric along the vertical axis. The fifth loading cycle was chosen for the purpose of demonstration because the weakest test section (i.e., the 300 mm UR_W section) failed after the fifth loading cycle. Only a small amount of compression was observed at a distance of 250 mm away from the center for all test sections except the 230 mm R_W and 150-mm-thick UR_M sections. These two sections showed a small amount of heave at 250 mm away from the center. All test sections constructed over the weak subgrade showed more compression at the center of the loading plate and more heave at 500 and 750 mm away from the center of the loading plate than the corresponding sections over the moderate subgrade. The unreinforced section showed more compression at the center and more heave at 500 and 750 mm away from the center than the corresponding reinforced sections. All test sections showed more heave at 500 mm away from the center of the loading plate than at 750 mm away from the center of loading plate. The thick sections had less heave and compression than the corresponding thin sections. The 300-mm-thick unreinforced base over the weak subgrade showed the largest amount of compression (i.e., 75.5 mm) and heave (i.e., 7.0 mm). Thakur et al. (2012) showed that the vertical stress at the interface of subgrade and base course decreased rapidly from 150 to 250 mm away from the center and then the stress decreased slowly with the farther distance. This stress distribution follows the typical layered elastic theory. Based on the stress-deformation relationship of a soil, the deformation is proportional to the stress, thus the observed surface permanent deformation satisfies this stress-deformation relationship. In addition, the permanent deformation beyond 250 mm away from the center was almost zero because this location was beyond the influence distance. The increase in the subgrade strength, the geocell reinforcement, and the base course thickness reduced the amount of surface heave and compression. This phenomenon can be justified by a beam on ground. According to the beam theory, hogging moment develops under the point of load application and sagging moment develops away from the point of load application. In addition, the subgrade under the load was compressed while the subgrade away from the center heaved. Thus, the largest compression was observed at the center of the loading plate and the largest heave was observed at the point away from the center of the loading plate.

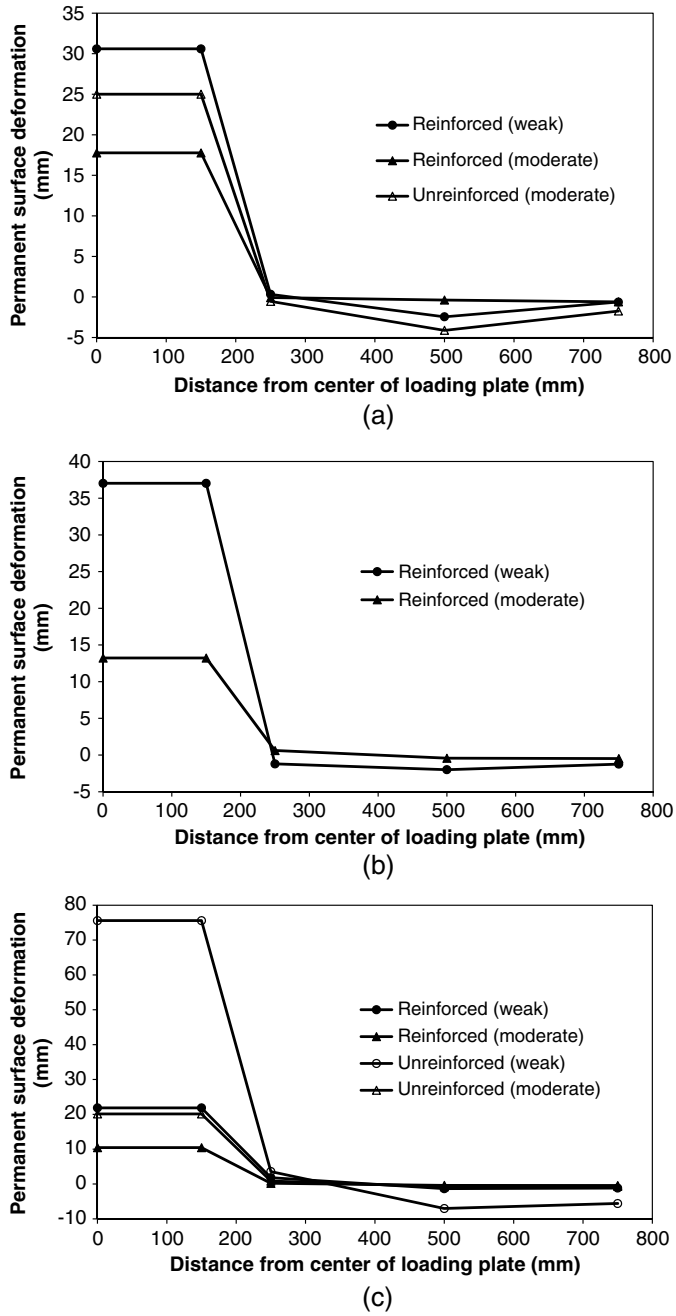

Fig. 11. Surface deformation profiles at the fifth loading cycle: (a) 150-mm-thick base; (b) 230-mm-thick base; (c) 300-mm-thick base

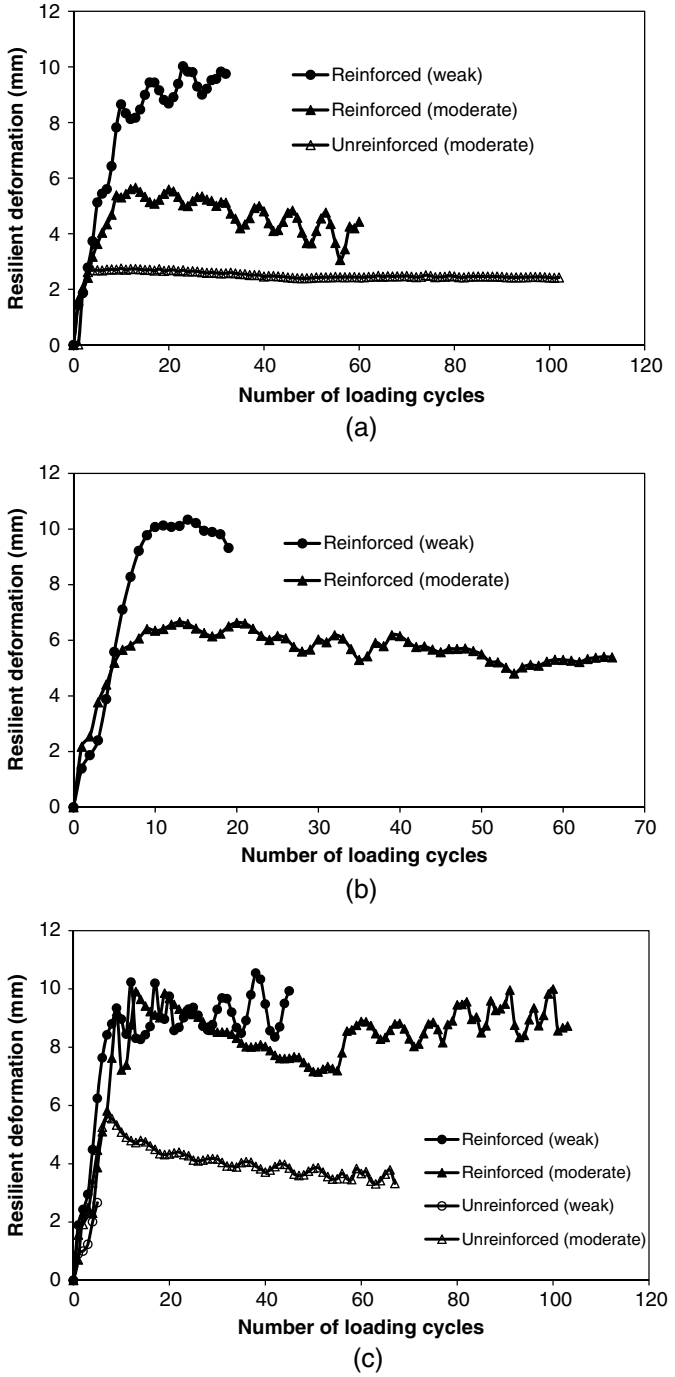

Fig. 12. Resilient deformation at the center of the loading plate versus the number of loading cycles: (a) 150-mm-thick base; (b) 230-mm-thick base; (c) 300-mm-thick base

Resilient Deformation

The resilient deformation is defined as the rebound deformation of a test section under cyclic loading and can be obtained when unloaded from the maximum load (40 kN) to the minimum load (0.5 kN). The resilient deformation at each loading cycle was calculated by deducting the permanent deformation from the total deformation at that cycle. The amount of the resilient deformation at each cycle was then divided by the total deformation at that cycle to obtain the percentage of resilient deformation. The resilient deformation and percentage of resilient deformation at the center of the loading plate versus the number of loading cycles are shown in Figs. 12 and 13, respectively. The amount of resilient deformation and the percentage of resilient deformation increased sharply for the first few loading cycles and stabilized to a nearly constant value for each test section except for the 300 mm UR_W section. All reinforced sections had more resilient deformation and a higher percentage of resilient deformation than the corresponding unreinforced sections. This improvement resulted from the slab effect and/or tensioned membrane effect by the geocell-reinforced layer, which is similar to a tensioned membrane effect by a planar reinforcement at a large deformation (Thakur et al. 2012). The reinforced sections constructed over the weak subgrade had more resilient deformation and a lower percentage of resilient deformation compared with those over the moderate subgrade. All reinforced sections constructed over the weak subgrade and the

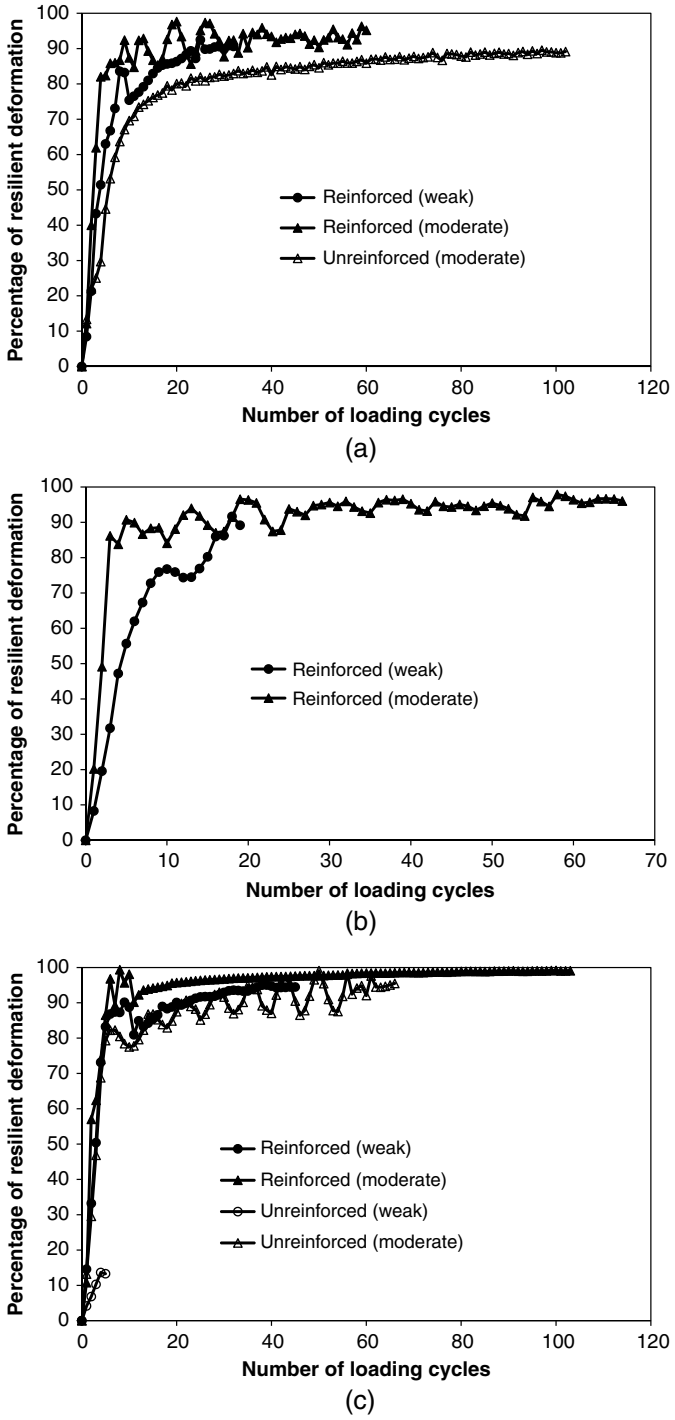

Fig. 13. Percentage of resilient deformation at the center of loading plate versus the number of loading cycles: (a) 150-mm-thick base; (b) 230-mm-thick base; (c) 300-mm-thick base

300 mm R_M section had approximately the same maximum resilient deformation (i.e., 10 mm). The 150 mm UR_M and the 300 mm UR_W sections had approximately the same maximum resilient deformation (i.e., 2.7 mm), while the 150 mm R_M, 230 mm R_M, and 300 mm R_M had approximately the same maximum resilient deformation (i.e., 6 mm). All test sections except for the 300 mm UR_W section shook down to a steady state showing resilient behavior. The 300 mm UR_W section did not shake down to a steady state and underwent continuous permanent deformation increase without showing much resilience. These results demonstrate that the geocell improved the resilient behavior of the RAP bases and the degree of improvement was higher for the sections over the weak subgrade than those over the moderate subgrade.

Conclusions

Nine large-scale laboratory cyclic plate loading tests were conducted on unreinforced and geocell-reinforced RAP bases with three different thicknesses (150, 230, and 300 mm) over weak and moderate subgrade to investigate the influence of geocell reinforcement, base course thickness, base course strength, and subgrade strength on the deformation behavior of RAP on the bases. The following conclusions can be made from this study:

- The amount and rate of the permanent deformation increased with the number of loading cycles;
- The geocell reinforcement improved the permanent deformation performance of the geocell-reinforced RAP bases by a factor of 1.1–11.4 as compared with the unreinforced bases;
- The increase of RAP base thickness by 150 mm improved the permanent deformation performance of the RAP base section by a factor of 1.1–2.7;
- The strengths of base course and subgrade layers influenced the performance of the RAP base sections;
- The increase of the subgrade CBR from 2 to 5% improved the permanent deformation performance of the RAP base sections by a factor of 1.2–17.2;
- The thicker unreinforced and reinforced sections performed better than the corresponding thinner sections, the reinforced sections performed better than the corresponding unreinforced sections, and the sections with high subgrade and base course strengths performed better than the corresponding sections with low subgrade and base course strengths;
- The increase in the subgrade strength, the geocell reinforcement, and the base course thickness reduced the amount of permanent surface compression and heave;
- The geocell improved the resilient behavior of the RAP bases and the degree of improvement was higher for the sections over the weak subgrade than those over the moderate subgrade; and
- The geocell-reinforced base sections and the base sections over the moderate subgrade showed a stable response, whereas the unreinforced base over the weak subgrade showed an unstable response.

Acknowledgments

This research was sponsored by the Mid-America Transportation Research Center. The Geosynthetic Institute (GSI) provided funding for the first author through the GSI Fellowship for conducting this research. The geocell material used in this research was provided by PRS Mediterranean, Ltd., in Israel. RAP materials were supplied by R.D. Johnson Excavating, Co. Mr. Howard Jim Weaver, the former laboratory manager, and Mr. Kahle Loveless and Mr. Aj Rahman, former undergraduate students in the Department of Civil, Environmental, and Architectural Engineering (CEAE) at the University of Kansas (KU) provided great assistance during the laboratory tests. The authors appreciate all this support.

References

Abdelrahman, M., Alam, T. B., Binte, T., and Zollars, J. (2010). "Performance of high recycled asphalt pavement (RAP) content as base layer in flexible pavement." *J. Solid Waste Technol. Manage.*, 36(3), 131–142.

Arulrajah, A., Rahman, M. A., Piratheepan, J., Bo, M. W., and Imteaz, M. A. (2014). "Evaluation of interface shear strength properties of geogrid-reinforced construction and demolition materials using a modified large-scale direct shear testing apparatus." *J. Mater. Civ. Eng.*, 10.1061/(ASCE)MT.1943-5533.0000897, 974–982.

ASTM. (2006). "Standard test methods for uncompacted void content of fine aggregate (as influenced by particle shape, surface texture, and grading)." *ASTM C1252–06*, West Conshohocken, PA.

ASTM. (2007a). "Standard test method for density and unit weight of soil in place by the sand-cone method." *ASTM D1556–07*, West Conshohocken, PA.

ASTM. (2007b). "Standard test method for density, relative density (specific gravity), and absorption of coarse aggregate." *ASTM C127–07*, West Conshohocken, PA.

ASTM. (2007c). "Standard test method for density, relative density (specific gravity), and absorption of fine aggregate." *ASTM C128–07a*, West Conshohocken, PA.

ASTM. (2009a). "Standard test method for accelerated tensile creep and creep-rupture of geosynthetic materials based on time-temperature superposition using the stepped isothermal method." *ASTM D6992*, West Conshohocken, PA.

ASTM. (2009b). "Standard test method for recovery of asphalt from solution by Abson method." *ASTM D1856–09*, West Conshohocken, PA.

ASTM. (2010). "Standard test method for asphalt content of hot-mix asphalt by ignition method." *ASTM D6307–10*, West Conshohocken, PA.

ASTM. (2011). "Standard test methods for quantitative extraction of bitumen from bituminous paving mixtures." *ASTM D2172/D2172M–11*, West Conshohocken, PA.

ASTM. (2013a). "Standard test method for bursting strength of textile fabrics Diaphragm bursting strength tester method." *ASTM D3786*, West Conshohocken, PA.

ASTM. (2013b). "Standard test method for index puncture resistance of geomembranes and related products." *ASTM D4883-07 e1*, West Conshohocken, PA.

ASTM. (2013c). "Standard test method for storage modulus calibration of dynamic mechanical analyzers." *ASTM E2254*, West Conshohocken, PA.

ASTM. (2014a). "Standard test method for linear thermal expansion of solid materials by thermomechanical analysis." *ASTM E831*, West Conshohocken, PA.

ASTM. (2014b). "Standard test method for oxidative-induction time of polyolefins by differential scanning calorimetry." *ASTM D3895*, West Conshohocken, PA.

ASTM. (2015a). "Standard test method for grab breaking load and elongation of geotextiles." *ASTM D4632*, West Conshohocken, PA.

ASTM. (2015b). "Standard test method for oxidative induction time of polyolefin geosynthetics by high pressure differential scanning calorimetry." *ASTM D5885*, West Conshohocken, PA.

ASTM. (2015c). "Standard test method for trapezoid tearing strength of geotextiles." *ASTM D4533*, West Conshohocken, PA.

ASTM. (2016a). "Standard test methods for determining apparent opening size of a geotextile." *ASTM D4751*, West Conshohocken, PA.

ASTM. (2016b). "Standard test methods for laboratory miniature vane shear test for saturated fine-grained clayey soil." *ASTM D4648*, West Conshohocken, PA.

ASTM. (2016c). "Standard test methods for water permeability of geotextile by permittivity." *ASTM D4491*, West Conshohocken, PA.

Attia, M.I.E.-S. (2010). "Characterization of the structural behavior of reclaimed asphalt pavement as pavement base layer." Ph.D. dissertation, Dept. of Civil Engineering, North Dakota State Univ., ProQuest, Ann Arbor, MI.

Bennert, T., and Maher, A. (2005). "The development of a performance specification for granular base and subbase material." *Rep. No. FHWA-NJ-2005-003*, Dept. of Transportation, Trenton, NJ.

Bennert, T. A., Papp, W. J., Jr., Maher, M. H., and Gucunski, N. (2000). "Utilization of construction and demolition debris under traffic-type loading in base and subbase applications." *Transp. Res. Rec.*, 1714, 33–39.

Bortz, B. S., Hossain, M., Halami, I., and Gisi, A. (2012). "Low-volume paved road improvement with geocell reinforcement." *Transportation Research Board Annual Meeting*, Transportation Research Board, Washington, DC.

Clary, J. A., DeGroot, D. J., and Highter, W. H. (1997). "Structural numbers for reclaimed asphalt pavement base and subbase course mixes." Dept. of Civil and Environmental Engineering, Univ. of Massachusetts, Amherst, MA.

Copeland, A., Jones, C., and Bukowski, J. (2010). "Reclaiming roads." ⟨http://www.fhwa.dot.gov/publications/publicroads/10mar/06.cfm⟩ (Nov. 2, 2010).

Cosentino, P. J., et al. (2012). "Improving the properties of reclaimed asphalt pavement for roadway base applications." *Rep. No. FL/DOT/BDK81-97702*, Florida Institute of Technology, Dept. of Civil Engineering, Florida Dept. of Transportation, Tallahassee, FL.

Dong, Q., and Huang, B. (2014). "Laboratory evaluation on resilient modulus and rate dependencies of RAP used as unbound base material." *J. Mater. Civ. Eng.*, 10.1061/(ASCE)MT.1943-5533.0000820, 379–383.

Garg, N, and Thompson, M. R. (1996). "Lincoln Avenue reclaimed asphalt pavement base project." *Transp. Res. Rec.*, 1547, 89–95.

Giroud, J. P., and Han, J. (2004a). "Design method for geogrid-reinforced unpaved roads. I: Development of design method." *J. Geotech. Geoenviron. Eng.*, 10.1061/(ASCE)1090-0241(2004)130:8(775), 775–786.

Giroud, J. P., and Han, J. (2004b). "Design method for geogrid-reinforced unpaved roads. II: Calibration of applications." *J. Geotech. Geoenviron. Eng.*, 10.1061/(ASCE)1090-0241(2004)130:8(787), 787–797.

Guthrie, W. S., Cooley, D., and Eggett, D. L. (2007). "Effects of reclaimed asphalt pavement on mechanical properties of base materials." *Transp. Res. Rec.*, 2005, 44–52.

Hammitt, G. M. (1974). "Thickness requirement for unsurfaced roads and airfields, bare base support." *Project 3782-65, Technical Rep. S-70-5*, US Army Engineer Waterways Experiment Station, Vicksburg, MS.

Han, J., et al. (2011). "Performance of geocell-reinforced RAP bases over weak subgrade under full-scale moving wheel loads." *J. Mater. Civ. Eng.*, 10.1061/(ASCE)MT.1943-5533.0000286, 1525–1534.

Han, J. (2015). *Principles and practice of ground improvement*, Wiley, Hoboken, NJ.

Han, J., Acharya, B., Thankur, J. K., and Parsons, R. L. (2012). "Onsite use of recycled asphalt pavement materials with geocells to reconstruct pavements damaged by heavy trucks." *Final Rep. No. 25-1121-0001-462*, Mid-America Transportation Center, Mid-America Transportation Center, Lincoln, NE.

Han, J., and Thakur, J. K. (2015). "Sustainable roadway construction using recycled aggregates with geosynthetics." *Sustainable Cities Soc.*, 14, 342–350.

ISO. (1999). "Determination of coefficient of linear thermal expansion and glass transition temperature." *ISO 11359-2*, Geneva.

ISO. (2006). "Determination of oxidation induction time of a polyolefin." *ISO 11357*, Geneva.

ISO. (2011). "Plastics—Determination of dynamic mechanical properties. Part 1: General principles." *ISO 6721-1*, Geneva.

Kim, W., and Labuz, J. F. (2007). "Resilient modulus and strength of base course with recycled bituminous material." *Rep. No. MN/RC-2007-05*, Minnesota Dept. of Transportation, Saint Paul, MN.

Li, L., Benson, C. H., Edil, T. B., Hatipoglu, B., and Onur, T. (2007). "Evaluation of recycled asphalt pavement material stabilized with fly ash." *Proc., Sessions of Geo-Denver 2007 Congress: Soil and Material inputs for Mechanistic-Empirical Pavement Design*, Vol. 169, Geo-Institute of ASCE, Reston, VA, 77–86.

Mohammadinia, A., Arulrajah, A., Sanjayan, J., Disfani, M. M., Bo, M. W., and Darmawan, S. (2014). "Laboratory evaluation of the use of cement-treated construction and demolition materials in pavement base and subbase applications." *J. Mater. Civ. Eng.*, 10.1061/(ASCE)MT.1943-5533.0001148, 04014186.

NAPA (National Asphalt Pavement Association). (2016). "Engineering overview." ⟨http://www.asphaltpavement.org/index.php?option=com_content&view=article&id=14&Itemid=33.⟩ (Sep. 6, 2016).

Papp, W. J., Jr., Maher, M. H., Bennert, T. A., and Gucunski, N. (1998). "Behavior of construction and demolition debris in base and subbase applications." *Proc., Sessions of Geo-Congress: Recycled Materials in Geotechnical Applications*, ASCE, Reston, VA, 122–136.

Pokharel, S., Han, J., Leshchinsky, D., Parsons, R. L., and Halahmi, I. (2010). "Investigation of factors influencing behavior of single geocell-reinforced bases under static loading." *Geotext. Geomembr.*, 28(6), 570–578.

Qian, Y., Han, J., Pokharel, S. K., and Parsons, R. L. (2011). "Stress analysis on triangular aperture geogrid-reinforced bases over weak subgrade under cyclic loading—An experimental study." *Transp. Res. Rec.*, 2204(2), 83–91.

Recycled Material Research Center. (2008). "User guideline for byproducts and secondary use materials in pavement construction." ⟨http://www.recycledmaterials.org/tools/uguidelines/rcc4.asp⟩ (May 24, 2012).

Taha, R., Ali, G., Basma, A., and Al-Turk, O. (1999). "Evaluation of reclaimed asphalt pavement aggregate in road base and subbase." *Transp. Res. Rec.*, 1652, 264–269.

Thakur, J. K., and Han, J. (2015). "Recent development of recycled asphalt pavement (RAP) bases treated for highway construction." *Transp. Infrastruct. Geotech.*, 2(2), 68–86.

Thakur, J. K., Han, J., and Parsons, R. L. (2013). "Creep behavior of geocell-reinforced recycled asphalt pavement (RAP) bases." *J. Mater. Civ. Eng.*, 10.1061/(ASCE)MT.1943-5533.0000705, 1533–1542.

Thakur, J. K., Han, J., Pokharel, S. K., and Parsons, R. L. (2012). "Performance of geocell-reinforced recycled asphalt pavement (RAP) bases over weak subgrade under cyclic plate loading." *Geotext. Geomembr.*, 35, 14–24.

Thompson, M. R., and Smith, K. L. (1990). "Repeated triaxial characterization of granular bases." *Transp. Res. Rec.*, 1278, 7–17.

Viyanant, C., Rathje, E. M., and Rauch, A. F. (2007). "Creep of compacted recycled asphalt pavement." *Can. Geotech. J.*, 44(6), 687–697.

Webster, S. L., Brown, R. W., and Porter, J. R. (1994). "Force projection site evaluation using the electric cone penetrometer (ECP) and the dynamic cone penetrometer (DCP)." *Technical Rep. GL-94-17*, U.S. Army Corps of Engineers, Washington, DC, 172.

Wen, H., Warner, J., Edil, T., and Wang, G. (2010). "Laboratory comparison of crushed aggregate and recycled pavement material with and without high carbon fly ash." *Geotech. Geol. Eng.*, 28(4), 405–411.

Wen, H., and Wu, M. (2011). "Evaluation of high percentage recycled asphalt pavement as base materials." *Rep. No. TNW2011-15*, U.S. Dept. of Transportation, Transportation Northwest Regional Center, Seattle.